Received: 18 January 2018 | Revised: 03 May 2018 | Accepted: 05 May 2018 | Published on: 16 October 2018

DOI: 10.1002/qj.3340

RESEARCH ARTICLE

Quarterly Journal of the Royal Meteorological Society RMetS

Analytical solution to a thermodynamic model for the sensitivity of afternoon deep convective initiation to the surface Bowen ratio

Mansi Bhowmick[1,2] | Douglas J. Parker[1]

[1]School of Earth and Environment, University of Leeds, Leeds, UK
[2]Centre for Atmospheric Science, Indian Institute of Technology, Delhi, India

Correspondence
Douglas J. Parker, School of Earth and Environment, University of Leeds, Leeds LS2 9JT, UK.
Email: d.j.parker@leeds.ac.uk

The tendency of convective rainfall to initiate over a wetter or drier land surface is a critical feedback process in the climate system, influencing the hydrological cycle on a variety of spatial scales, especially in parts of the world where water is limited. A simple algebraic solution is derived from fundamental physical equations, to predict the sign of this convective rainfall feedback with the surface. The tendency for convection to occur is evaluated by the rate at which the convective boundary-layer top approaches the level of free convection. Well-known integral models predict the rate of ascent of the boundary-layer top, which tends to be faster over a dry surface. The associated changes in equivalent potential temperature in the boundary layer determine the rate at which the level of free convection descends, typically faster over a wet surface, as a function of the ambient profile, the thermodynamic forcing and the surface Bowen ratio. The resulting system is controlled by three parameters. Two nondimensional parameters determine whether there is wet or dry "advantage"; the Bowen ratio at the boundary-layer top and a "convective instability parameter," defined as the ratio of the vertical gradient of saturated equivalent potential temperature at the level of free convection to the profile stability just above the boundary layer. A dimensional function, dependent on the surface fluxes, the boundary-layer depth, and the profile stability, provides the magnitude of the response. In comparison with previous work, the solution is both rigorously derived from physical principles and encapsulated in a simple algebraic form. A first evaluation of the theoretical framework has been made using data from a convection-permitting numerical model simulation over India, and this indicates that the equations successfully determine the conditions under which convection is triggered over dry surfaces.

KEYWORDS

Bowen ratio, convection, convective boundary layer, convective initiation, cumulonimbus, land–atmosphere interaction, mixed-layer model, precipitation, rainfall

1 | INTRODUCTION

Over recent decades, it has increasingly become clear that soil moisture conditions can control the initiation of deep convection, and hence control rainfall. A number of observational and modelling studies have demonstrated the links between the surface moisture state and cumulus convective rainfall (for example, Cutrim *et al.*, 1995; Pielke *et al.*, 1997; Trier *et al.*, 2004; Taylor and Ellis, 2006; Taylor *et al.*, 2007; Wang *et al.*, 2009; Garcia-Carreras *et al.*, 2010; Guillod *et al.*, 2014). More generally, variability in land surface temperature (Taylor *et al.*, 2012) is significantly related to afternoon rainfall worldwide.

Several studies have attempted to explain the relationships and feedbacks between the surface state and the rainfall (for example, Eltahir, 1998; Peilke, 2001; Daly *et al.*, 2004; Ek

and Holstag, 2004; Huang and Margulis, 2011). Although surface roughness and surface albedo both influence the boundary-layer state and therefore influence the conditions supplying rainfall, most attention has focussed on the role of spatial patterns in soil moisture (for example, Pielke *et al.*, 1991; Chen and Avissar, 1994; Schär *et al.*, 1999; Findell and Eltahir, 2003a; Taylor *et al.*, 2011; Huang and Margulis, 2012; Gentine *et al.*, 2013; Lintner *et al.*, 2013; Guillod *et al.*, 2015), which affects the partitioning of the latent heat flux and sensible heat flux and thus the surface Bowen ratio. Increased vegetation cover and increased soil moisture each act to reduce the Bowen ratio. If afternoon convection is more likely to be triggered over such a vegetated or wet surface, there is said to be "wet advantage" (or positive feedback), whereas "dry advantage" (negative feedback) refers to conditions in which afternoon convection is more likely over a surface of high Bowen ratio, where there are conditions of low evaporation.

Considerable progress has been made in understanding the response of the boundary layer to the Bowen ratio in different atmospheric profiles (Haiden, 1997; Findell and Eltahir, 2003; Huang and Margulis, 2011), using one-dimensional models. Such models consider the growth of the boundary layer in height and the evolution of its thermodynamic properties to determine whether these changes favour the release of moist conditional instability and deep convection over a given surface. These one-dimensional models do not consider dynamic triggering of the convection by vertical circulations, which are generally two- or three-dimensional (Birch *et al.*, 2014), but they may tell us whether convection is more strongly favoured on one day rather than another (for instance, according to changes in the profile and the surface state) or whether convection may be favoured over one surface or another, in conditions when dynamic forcing is weak. Guillod *et al.* (2015) have shown how soil-moisture feedbacks with rainfall on the (spatial) mesoscale can be dominated by dry-advantage feedbacks, while temporal relationships are dominated by wet advantage, indicating that there is value in studying the spatial and temporal relationships independently. The conceptual simplicity of one-dimensional models makes them attractive for the development of physical understanding of the problem.

Haiden (1997) addressed the question of cumulus formation by solving a boundary-layer evolution equation analytically, to assess the point at which the equilibrium height of boundary-layer air reaches the lifting condensation level (LCL). Haiden (1997) showed an interesting sensitivity of the cumulus onset to the surface Bowen ratio and stability above the boundary layer, with the sensitivity to the Bowen ratio changing sign according to the stability of the profile. Similarly, Ek and Holtslag (2004), in discussing the evolution of boundary-layer cloud, used theory, observations, and models to show that the stability and dryness just above the boundary layer are both important in the sign of the response to soil moisture. A regime exists, with low stability and reasonably humid air above the boundary layer, in which cloud cover can be suppressed by surface moisture (Huang and Margulis, 2011). These studies of shallow cumulus development do not necessarily apply to deep convective initiation, since the behaviour of the LCL and the level of free convection (LFC) differ significantly and may have opposite tendencies. Parker (2002) analysed the tendencies in convective available potential energy and convective inhibition (CAPE and CIN) according to the surface Bowen ratio and atmospheric stability, but failed to synthesise these results in a manner that would enable the question of wet or dry advantage to be answered.

Findell and Eltahir (2003, hereafter FE03a) made a number of innovations that enable the deep convective initiation problem to be understood physically and quantitatively. FE03a contrasted surface states of low and high Bowen ratio and considered the mechanisms by which the boundary-layer depth and the level of free convection move closer together, to a point at which CIN is very low and deep convective initiation is presumed to occur. Over a wet surface of low Bowen ratio, the boundary-layer growth is always relatively slow, because the sensible heat flux is relatively low, and therefore over the wet surface the approach of conditions of deep convection occurs by descent of the LFC (as the assumed cloud parcel from the boundary layer increases its equivalent potential temperature). In contrast, over a dry surface of high Bowen ratio, the boundary-layer depth can increase much more rapidly, and this rate of increase depends on the stability of the profile just above the capping inversion (quantified by FE03a as a convective triggering potential, or CTP, which is inversely related to the stability). In conditions where that stability is low (CTP is high), the dry boundary layer grows rapidly and may approach the LFC. On the basis of this conceptual model, FE03a argued that the occurrence of wet or dry advantage is controlled by two parameters, namely CTP and a humidity index, HI, defined as the sum of dewpoint depressions at 50 and 100 hPa above the ground. Using a one-dimensional numerical model, FE03a plotted the occurrence of wet and dry advantage on axes of CTP and HI, to argue finally that certain regions of (CTP, HI) space can be used to determine the likely behaviour. This approach has been quite influential and has been applied in a number of contexts. Tuinenburg *et al.* (2011) used the same (FE03a) slab model along with radiosonde observations over India to study local land–atmosphere feedbacks and proposed modified thresholds for CTP and HI. Ferguson and Wood (2011) used satellite remote sensing and reanalysis data to derive a modified CTP–HI framework to study soil moisture–precipitation feedback globally.

Although the CTP–HI approach of FE03a brings in some useful innovations, helping us to understand the problem, it also has some drawbacks. Primarily, it is not clear why these two parameters are thought to be the right ones (and the only ones) to characterize the conditions. The role of CTP in allowing a dry boundary layer to grow rapidly can be understood physically, but the dependence on HI is not obvious. In fact, observations (Parsons *et al.*, 2000) and models of

boundary-layer growth (for example, Betts and Ball, 1995; Parker, 2002) emphasize the role of dry air above the boundary layer in controlling the likelihood of deep convection, implying that a measure of this dryness, such as the difference in humidity between the boundary layer and the layer above, should be used. Furthermore, there have been questions over the generality of the results: FE03a tested their model with profiles typical of the continental United States, but when it was applied to Indian profiles, Tuinenburg *et al.* (2011) found higher values of CTP–HI to be required to reduce the prediction error of the framework. On the other hand, Ferguson and Wood (2011) found that the fixed threshold framework of F03a cannot be applied at a global scale and required a modified framework including latitudinally variable, zonal CTP–HI thresholds calculated at 5° intervals. This apparent lack of generality suggests that either additional parameters are needed to characterize the problem or the two parameters chosen are not the optimal ones.

Articles by Gentine *et al.* (2013) and Yin *et al.* (2015) both provide direct calculations of the evolution of the deep convective state of a one-dimensional atmospheric profile over surfaces of differing surface Bowen ratio. Gentine *et al.* (2013) analysed the shallow convection problem, but also calculated the buoyancy of boundary-layer air relative to the air just above the boundary layer, as a measure of CIN, to assess the possibility of free convection. In contrast, Yin *et al.* (2015) made numerical calculations of the CAPE of boundary-layer air at the time when the boundary-layer depth reaches the LCL. Each of these articles was able to show, directly from the simple physical basis model, quantitative estimates of the conditions separating wet and dry advantage as a function of the atmospheric temperature and humidity profile and the surface conditions.

Here, we redevelop the FE03a model from first principles, using the theoretical boundary-layer growth model of Betts (1973), Carson (1973), and Tennekes (1973), which has previously been used in the convective initiation problem by Haiden (1997), Parker (2002), Gentine *et al.* (2013), and Yin *et al.* (2015). We take a different approach from those earlier articles in the way that we analyse the conditions for deep convection, and this approach leads to simpler analytical and graphical solutions. It will be shown that the model can be solved exactly, to yield the three parameters that are needed to establish whether wet or dry advantage will occur in given conditions.

2 | DEVELOPMENT OF THE ONE-DIMENSIONAL MODEL

It is the goal of this article to describe the likelihood of a given atmospheric profile supporting deep, as opposed to shallow, convection. Specification of the conditions for deep convection to occur can be approached in different ways. For example, Gentine *et al.* (2013) estimated the CIN of boundary-layer air relative to air above the boundary layer, while Yin *et al.* (2015) computed the CAPE at the time of 'crossing the LCL' as different measures of the likelihood of deep convection. Instead, here we follow the approach of FE03a in considering deep convection to become more likely as the top of the boundary layer approaches the LFC, and use the rates at which these levels approach each other to differentiate wet and dry advantage. Like FE03a, we assume that a morning atmospheric sounding can be analysed to explain the forthcoming tendencies in the boundary-layer state and LFC over surfaces of differing wetness.

TABLE 1 Symbols used in the analysis

Symbol	Description
P_i	pressure depth of mixed layer
p_s	surface pressure
p_F	pressure at level of free convection (LFC)
Δp	pressure difference between inversion and LFC, $p_s - p_F$
z_i	inversion height above ground
R	rate of change of Δp, or convective triggering rate
R_1	convective triggering rate parameter
ΔR	difference in R between wet and dry surface conditions
θ_e	equivalent potential temperature
θ_{es}	saturated equivalent potential temperature
F_n	net surface heat flux
β	surface Bowen ratio
β_i	inversion Bowen ratio
β_v	slope of dry virtual adiabat
A_R	entrainment parameter
Γ_+	stability of profile just above boundary-layer capping inversion
S_F	conditional instability at the LFC
a	nondimensional parameter in rate equation
b	nondimensional parameter in rate equation
σ	convective instability parameter, S_F/Γ_+
r_s	saturation humidity mixing ratio
Γ	thermodynamic stability of profile

Following Betts (1992) and Betts and Ball (1995), we define the pressure depth of the mixed layer to be

$$P_i = p_s - p(z_i), \tag{1}$$

where z_i is the inversion height, $p(z)$ is the pressure as a function of height, and p_s is the surface pressure. Symbols used here and elsewhere in the article are listed in Table 1. The pressure difference between the inversion and the level of free convection, p_F, is

$$\Delta p = p(z_i) - p_F \tag{2}$$

(Figure 1). The rate of change of Δp with time, or "convective triggering rate," R, can be defined as

$$R \equiv \frac{d\Delta p}{dt} = -\frac{dP_i}{dt} - \frac{dp_F}{dt}, \tag{3}$$

where we assume that the temporal variation of surface pressure is small relative to the other terms. For a transition to deep convection by one-dimensional boundary-layer growth,

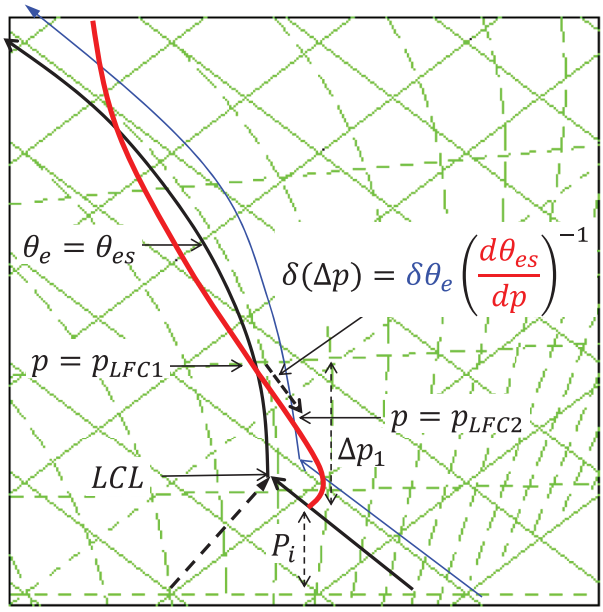

FIGURE 1 Schematic thermodynamic diagram (tephigram) showing the assumed structure of the atmospheric profile. The black and red lines indicate the parcel ascent and environmental profiles, respectively, and the level of free convection (LFC) lies at their intersection. If the boundary-layer equivalent potential temperature, θ_e, increases by an amount $\delta\theta_e$, the new parcel ascent is indicated by the blue curve and the LFC correspondingly descends, as indicated by the black dashed arrow. The resulting change in the level of free convection (LFC), which causes a change in Δp, is then inversely proportional to the gradient of saturated equivalent potential temperature, θ_{es} in the environmental profile, at the LFC (see text for more details)

we require that the LFC and inversion approach each other, and that $R < 0$.

The first term in Equation 3, along with the tendency in potential temperature, θ, can be calculated with good accuracy using well-known bulk formulae for the growth of a convective boundary layer (Betts,1973; Carson, 1973; Tennekes, 1973). The main assumption in this model is that the turbulent heat flux due to entrainment at the boundary-layer inversion is a constant fraction, A_R, of the surface sensible heat flux. Here we use the model in the form given by Betts and Ball (1995):

$$\frac{d\theta}{dt} = \frac{gF_n\beta}{c_p P_i(\beta+1)}\left[1 + \frac{\beta_i}{\beta}A_R\frac{(\beta-\beta_v)}{(\beta_i-\beta_v)}\right], \tag{4}$$

$$\frac{dP_i}{dt} = \frac{1}{\Gamma_+}\frac{d\theta}{dt}, \tag{5}$$

where

$$\Gamma_+ = -\left.\frac{d\theta}{dp}\right|_+ \tag{6}$$

is the stability of the profile just above the boundary-layer capping inversion, g the acceleration due to gravity, F_n the net surface heat flux (the net radiative and ground heat fluxes, corresponding to the total sensible and latent heat flux into the atmosphere through the surface energy balance), β the surface Bowen ratio, c_p the specific heat at constant pressure, A_R the entrainment parameter, and $\beta_v \approx -0.07$ the slope of the dry virtual adiabat (Betts, 1992). These equations have been found in many studies to have useful accuracy in describing the daytime growth of convective boundary layers. The second term in parentheses in Equation 4 is the one representing the entrainment assumption at the boundary-layer top. A_R is thought to have a value of between 0.2 and 0.4, and probably depends in practice on the presence of wind shear or shallow cumulus. Here we will assume that A_R is a constant. We note that, in normal circumstances, $\Gamma_+ > 0$.

Most commonly, β_i is negative, with boundary-layer growth corresponding to dry entrainment and the sensible and latent heat fluxes at the boundary layer inversion being of opposite sign. On relatively rare occasions it is possible to observe $\beta_i > 0$, when there is particularly humid air lying above the boundary layer (for example, LeMone *et al.*, 2000). The right-hand side of Equation 4 has a singularity at $\beta_i = \beta_v$: this corresponds to the situation in which the boundary-layer inversion corresponds to a virtual adiabat (Betts, 1992). Therefore we expect $\beta_v < \beta_i < 0$ not to occur, on physical grounds; in this regime, the inversion would be unstable in terms of θ_v. At this point it is worth noting that it would be possible to make the approximation $\beta_v = 0$, thereby removing the singularity from the equations and somewhat simplifying the algebra. This approximation amounts to ignoring the effect of moisture on buoyancy around the boundary-layer inversion level and, given the other approximations used (such as the uncertainty in A_R), it arguably does not lead to a large error. However, given that we are able to obtain a closed algebraic solution anyway, we do not make the $\beta_v = 0$ approximation here.

The second term on the right-hand side of Equation 3 can be related to the development of equivalent potential temperature in the boundary layer by inspection of the parcel ascent curve in the vicinity of the LFC. From Figure 1, in which we assume that the parcel equivalent potential temperature, θ_e, is equal to that of the well-mixed boundary layer, it can be seen that

$$\frac{dp_F}{dt} = \frac{\left.\frac{d\theta_e}{dt}\right|_{PBL}}{\left.\frac{d\theta_{es}}{dp}\right|_{LFC}} \tag{7}$$

and we can use

$$\left.\frac{d\theta_e}{dt}\right|_{PBL} = \frac{gF_n}{c_p P_i}\left[1 + A_R\frac{(\beta_i+1)}{(\beta+1)}\frac{(\beta-\beta_v)}{(\beta_i-\beta_v)}\right] \tag{8}$$

(Betts and Ball 1995) to obtain

$$\frac{dp_F}{dt} = \frac{gF_n}{S_F c_p P_i}\left[1 + A_R\frac{(\beta_i+1)}{(\beta+1)}\frac{(\beta-\beta_v)}{(\beta_i-\beta_v)}\right], \tag{9}$$

in which

$$S_F \equiv \left.\frac{d\theta_{es}}{dp}\right|_{LFC} \tag{10}$$

is a measure of the conditional instability of the profile. For a conditionally unstable atmosphere in which convective showers may occur, we require $S_F > 0$. Putting Equations 4, 5 and

9 in Equation 3 yields

$$R = -\frac{gF_n\beta}{\Gamma_+ c_p P_i(\beta+1)}\left[1+\frac{\beta_i}{\beta}A_R\frac{(\beta-\beta_v)}{(\beta_i-\beta_v)}\right] - \frac{gF_n}{S_F c_p P_i}\left[1+A_R\frac{(\beta_i+1)}{(\beta+1)}\frac{(\beta-\beta_v)}{(\beta_i-\beta_v)}\right]. \quad (11)$$

In this one-dimensional model, the question of whether a given atmospheric profile offers a wet or dry advantage in terms of convective initiation comes down to a question of whether the rate of change of pressure difference between the top of the boundary layer and LFC, R, is higher over a wet (low β) or dry (high β) surface. Given that R is negative if any initiation is to occur, wet advantage implies that R is an increasing function of β, or $dR/d\beta > 0$, and dry advantage occurs when R decreases with β, or $dR/d\beta < 0$.

Equation 11 can now be rearranged in the following form, to clarify the dependence on β:

$$R = R_1\frac{b\beta - a}{1+\beta}, \quad (12)$$

where a, b and R_1 are all independent of β. The nondimensional parameters a and b are given by

$$a = -\beta_i A_r\frac{\beta_v}{\beta_i-\beta_v} + \frac{1}{\sigma}\left(1 - A_r\beta_v\frac{\beta_i+1}{\beta_i-\beta_v}\right) \quad (13)$$

and

$$b = -1 - A_r\frac{\beta_i}{\beta_i-\beta_v} - \frac{1}{\sigma}\left(1+A_r\frac{\beta_i+1}{\beta_i-\beta_v}\right), \quad (14)$$

where

$$\sigma = \frac{S_F}{\Gamma_+}. \quad (15)$$

σ will be termed the "convective instability parameter", because S_F is a measure of the conditional instability and Γ_+ is the profile stability just above the boundary layer (to be discussed in more detail later). The rate parameter, R_1, is the only dimensional quantity on the right-hand side of Equation 12 and it is positive-definite:

$$R_1 = \frac{gF_n}{\Gamma_+ c_p P_i}. \quad (16)$$

R_1, like R, has units of Pa/s.

To establish the dependence of R on surface state, we differentiate R with respect to β, from Equation 12, to find

$$\frac{dR}{d\beta} = R_1\frac{b+a}{(1+\beta)^2}. \quad (17)$$

Equation 17 tells us that the sign of $dR/d\beta$ is independent of β itself. This is a powerful result, because it means that the question of wet or dry advantage is universal in terms of surface Bowen ratio; its sign is independent of Bowen ratio. This is in contrast to the shallow-cumulus system explored by Gentine *et al.* (2013), for which the sensitivity of the inversion-level relative humidity to the evaporative fraction, EF, changes sign according to EF, leading to a rather complicated set of possibilities. Furthermore, since R_1 is a positive-definite function in convective conditions, the sign of $dR/d\beta$ (and hence the separatrix between wet and dry advantage, $dR/d\beta = 0$) is determined by the sign of $b+a$. If $b+a > 0$ then we expect wet advantage and if $b+a < 0$ we expect dry advantage.

Once it is seen that the function $R(\beta)$ is monotonic, the question of wet or dry advantage can alternatively be found by comparing the wet (low β) and dry (high β) limits of R. These are, respectively,

$$R(0) = -R_1 a, \quad (18)$$

$$R(\infty) = R_1 b, \quad (19)$$

and the difference in R between dry and wet conditions is

$$\Delta R = R_1(b+a). \quad (20)$$

Again, the conclusion is reached that the sensitivity of R to β is controlled by R_1 and $(b+a)$, with $(b+a)$ alone determining the sign of ΔR. Henceforth, we use ΔR to assess the sign and amplitude of the sensitivity of convective initiation to the surface Bowen ratio.

Expanding b and a yields

$$b+a = -1 - A_r\beta_i\frac{\beta_v+1}{\beta_i-\beta_v} - \frac{1}{\sigma}A_r(\beta_i+1)\frac{\beta_v+1}{\beta_i-\beta_v} \quad (21)$$

and, if we were to make the assumption $\beta_v = 0$ (ignoring the buoyancy effects of moisture as discussed above), this would simplify to

$$b+a = -1 - A_r\left(1+\frac{\beta_i+1}{\sigma\beta_i}\right). \quad (22)$$

Putting the complete form, Equation 21, back into Equation 17 gives

$$\frac{dR}{d\beta} = \frac{\Delta R}{(1+\beta)^2} = -\frac{R_1}{(1+\beta)^2} \times\left\{1 + A_r\beta_i\frac{\beta_v+1}{\beta_i-\beta_v} + \frac{1}{\sigma}A_r(\beta_i+1)\frac{\beta_v+1}{\beta_i-\beta_v}\right\}.$$

Unlike FE03a, who identified two parameters (CTP and HI) to categorize the behaviour of the system, we find that the progression of the boundary layer towards triggering over surfaces of differing Bowen ratio is controlled by three parameters derived from the ambient profile, namely β_i and σ (which together control b and a) and R_1 (which is the only dimensional parameter involved). We are fortunate that the separatrix between wet and dry advantage given by $b+a=0$ depends only on two of these parameters, β_i and σ, and is independent of R_1.

3 | SENSITIVITY OF CONVECTIVE DEVELOPMENT FUNCTIONS, R AND ΔR, TO CONTROLLING PARAMETERS

3.1 | Summary of the controlling parameters

The strength of the gradient of R with β, ΔR, which quantifies the degree of wet or dry advantage, depends only on the functions a, b and R_1. Since R_1 is positive-definite, this reduces to two statements.

- $b+a$ determines the sign of ΔR, and therefore controls wet or dry advantage. This depends only on β_i and σ.
- $\Delta R = R_1(b+a)$ determines the amplitude of the sensitivity, and depends on all three parameters, β_i, σ, and R_1.

3.2 | Typical values and functional forms

Making sense of these relationships requires some appreciation of physically relevant values of the external parameters. The inversion-level Bowen ratio can be estimated in terms of the humidity and temperature jumps across the boundary-layer inversion, according to

$$\beta_i = \frac{c_p}{L}\frac{\delta\theta}{\delta q}, \tag{23}$$

where L is the latent heat of vaporization and q the mixing ratio. Betts and Ball (1995), in presenting data from the First International Land Surface Climatology Project Field Experiment (FIFE), suggest that β_i may take a wide range of values, though for most of FIFE β_i lay in the range $-0.5 < \beta_i < -0.3$. For physical reasons, we require $\beta_i < \beta_v \sim -0.07$ or $\beta_i > 0$.

The stability just above the boundary-layer inversion, Γ_+, may take a wide range of values, from very low stability associated with a residual boundary layer to stable values associated with subsidence. High values might correspond to an isothermal layer, which close to the ground would have a stability of the order of $\Gamma_+ \sim g/c_p \sim 10^{-3}$ K/Pa.

In deep convective conditions, S_F can also take a wide range of values. Starting from a definition of saturated equivalent temperature in the form

$$c_p\frac{d\theta_{es}}{\theta_{es}} = c_p\frac{d\theta}{\theta} + d\left(\frac{Lr_s}{T}\right) \tag{24}$$

(where r_s is the saturation humidity mixing ratio) and approximating L as a constant, the direct relationship between a profile's thermodynamic gradients

$$S = \frac{d\theta_{es}}{dp} \qquad \text{and} \qquad \Gamma = -\frac{d\theta}{dp}$$

can be found, in the form

$$S = -\Gamma\left.\frac{\partial\theta_{es}}{\partial\theta}\right|_p + \left.\frac{\partial\theta_{es}}{\partial p}\right|_\theta, \tag{25}$$

where

$$\left.\frac{\partial\theta_{es}}{\partial\theta}\right|_p = \frac{\theta_{es}}{\theta}\left[1 + \frac{Lr_s}{c_pT}\left(\frac{L}{R_vT} - 1\right)\right], \tag{26}$$

$$\left.\frac{\partial\theta_{es}}{\partial p}\right|_\theta = \theta_{es}\frac{Lr_s}{pc_pT}\left[\left(\frac{L}{R_vT} - 1\right)\frac{R_a}{c_p} - 1\right], \tag{27}$$

and R_a and R_v are the gas constants for air and water vapour, respectively. Larger values of S_F are obtained for warm tropical environments and are maximized when Γ at the same level is almost zero. For example, at a pressure of 750 hPa and $\theta = 320$ K, the magnitude of S_F is a maximum of 3.7×10^{-3} K/Pa when $\Gamma = 0$. At cooler temperatures, S_F is much smaller.

The convective instability parameter, $\sigma = S_F/\Gamma_+$, has a reasonably straightforward relationship with the lower tropospheric stratification, because S_F decreases with Γ_F (evaluated at the LFC) in conditionally unstable conditions. This relationship can be inferred from Equation 25 or from inspection of a tephigram, where a profile with low Γ_F has strong conditional instability (high S_F). In consequence, σ decreases with both increasing Γ_F and Γ_+. When Γ_F and Γ_+ are high and the lower troposphere is stable (a warm mid-troposphere), σ will be low. High σ means a more unstable lower troposphere and cool mid-troposphere. For this reason, the convective instability parameter, σ, can be viewed as a measure of lower tropospheric instability and will be similar in functional behaviour to the CTP defined by FE03a.

In comparing the likely values of Γ_+ and S_F, it appears that σ ranges from much less than 1 to values that can be much higher than 10. However, it should also be recognized that very low values of σ are unlikely to have CAPE, because the combined condition of high Γ_+ and low S_F corresponds to a very warm mid-troposphere. For this reason, very low σ corresponds to a profile that is too stable for deep convection. The particular thresholds over which deep convection is possible will depend on the climatological conditions, since the relationships between θ_{es} and θ are sensitive to pressure and temperature and will need to be tested in practice.

R_1, as the only dimensional parameter in the system, controls the absolute magnitude of the response to the surface. In understanding the physical meaning of this parameter, it can be seen that it is proportional to the net surface heat flux and inversely proportional to the boundary-layer depth and the stability just above the boundary layer. Strong surface fluxes lead to rapid boundary-layer growth, but this growth is "diluted" if the boundary layer is deep and suppressed if the stability is high. R_1 is therefore the primary control on the rate of boundary-layer growth, whether over a wet or dry surface. In order to estimate typical scales of the response in terms of the amplitude of R_1, it is helpful to note that we can use the hydrostatic relation to approximate $P_i/z_i \sim \rho g$, and therefore write

$$R_1 = \frac{F_n}{\rho c_p\Gamma_+ z_i}, \tag{28}$$

where z_i is the boundary-layer inversion height. Given that, for an isothermal layer, the stability is approximately

$$\Gamma \equiv \frac{d\theta}{dz} \approx \frac{g}{c_p}, \tag{29}$$

$g/(c_p\Gamma_+)$ is likely to be greater than 1 for profiles supporting deep convection, because an isothermal layer represents a reasonably strong stability above the boundary-layer inversion. With strong surface fluxes ($F_n \sim 500$ Wm^{-2}) over a shallow PBL ($z_i \sim 500$ m), typical values of R_1 may be of the order $R_1 \sim 0.1$ Pa/s, but can range from just above zero (at sunrise when the net heat flux is low) to much greater than 1 Pa/s if P_i and Γ_+ are small. Note that a value of $R \sim -1$ Pa/s would be a reasonably rapid rate of decrease of Δp, about 360 m/hr using a hydrostatic approximation of 10 Pa/m. The results of the evaluation of the model against numerical

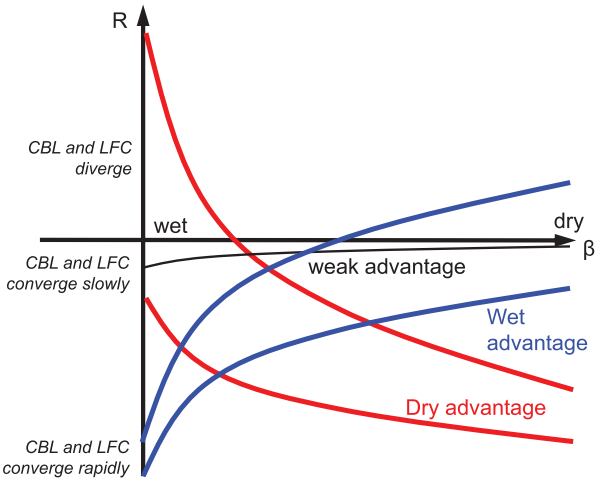

FIGURE 2 Typical curves of R as a function of surface Bowen ratio, β, for wet and dry advantage, as given by Equation 12. The atmosphere moves more rapidly towards deep convective initiation when R is strongly negative, therefore curves for which R is strongly negative at lower values of β (blue curves) show wet advantage. Similarly, curves for which R is more negative for large β (red curves) have dry advantage. Solutions with small values of R show only weak wet or dry advantage. Note that the limiting values of each curve are related to the parameters a, b and R_1 by $R(0) = -R_1 a$, and $R(\infty) = R_1 b$

model simulation data (Section 5) confirm that significant values of R_1 of the order $R_1 \sim 0.1$ Pa/s are indeed obtained.

Now, considering Equations 12 and 17, it can be seen that the shape of $R(\beta)$ is relatively simple, as illustrated by Figure 2. From consideration of Figure 2, we can summarize the conditions for wet or dry advantage as follows.

- If $\Delta R = R_1(b+a)$ is small, then there is no significant wet or dry advantage (illustrated in Figure 2 by a grey curve).
- If $\Delta R = R_1(b+a)$ is not small, and R is negative for some β, then
  - if $b + a > 0$ there is wet advantage (blue curves);
  - if $b + a < 0$ there is dry advantage (red curves).

The numerical evaluation of these rules can be seen in Figure 3, in which ΔR is plotted as a function of (β_i , σ) for two different values of Γ_+. Note that the separatrix between wet and dry advantage is the same curve in each panel of Figure 3; only the amplitudes of the wet and dry responses in each regime of the plot change, according to the differing Γ_+, and therefore R_1, in each. The horizontal β_i axis delineates the control by the inversion Bowen ratio. Most commonly, atmospheric profiles lie in the negative β_i regime, where large negative values mean that the humidity gradient at the inversion is weak, but low negative values imply a strong gradient at the inversion, with dry air above the boundary layer. The vertical σ axis quantifies the lower tropospheric instability: as noted earlier, given that the static stability at the LFC, Γ_F, and conditional instability, S_F, tend to be oppositely related, $\sigma = S_F/\Gamma_+$ will tend to be inversely proportional to lower tropospheric stability and proportional to FE03a's CTP. In Figure 3a, corresponding to low stability and rapid boundary-layer growth, the regime appears to be dominated by high dry advantage for high σ and strongly negative β_i. In contrast, in Figure 3b, which corresponds to a relatively stable, isothermal layer above the boundary layer, dry advantage is weaker and very high values of wet advantage appear to be possible. Note, however, that a logarithmic scale is used in Figure 3, and the low values of σ that dominate Figure 3b may correspond to atmospheric profiles that are too stable for deep convection. In both panels of Figure 3, the regime of positive β_i corresponds to strong dry advantage.

From inspection of Figure 3 and consideration of Equation 17, the sensitivity of triggering to surface type and atmospheric profile can be explained in the following ways.

3.3 | Physical interpretation of the controls on wet and dry advantage

If it is the case that R is sufficiently large and negative for one-dimensional triggering to be a possibility, then we can consider the conditions that determine the sign of $(b + a)$ in Equation 17 as a function of just two parameters: β_i and σ.

The inversion Bowen ratio, β_i, controls the rate of drying of PBL air by entrainment and, in most circumstances, where the air above the PBL is drier than the air in the PBL, this drying tends to reduce θ_e (slows its increase due to surface sensible and latent heating) and therefore restricts the rate of descent of p_F. For these reasons, the PBL over the dry surface normally has lower θ_e than the air over the wet surface and, in extreme cases, θ_e can fall with time over the dry (Betts and Ball, 1995; Rochetin *et al.*, 2017, their fig. 7). Whether this process is significant depends then on the difference in humidity between the PBL and the air above it (not, as in FE03a, a sum of low-level humidities, HI). When the humidity difference between PBL air and the air above is small, β_i is very large and negative and we should expect a dry advantage: the LFC behaves similarly over the wet and dry ground, because there is little reduction of θ_e due to entrainment, and p_F is similar over the wet and dry surfaces, but the boundary layer grows deeper more rapidly over the dry surface. In contrast, when the difference in humidity between the PBL and the air above it is large, β_i is very small and negative and θ_e in the PBL is significantly reduced by entrainment. In this case, while the boundary layer over the dry surface may be deepening rapidly, p_F over this surface may also be rising less rapidly (or even possibly falling) relative to p_F over the wet surface, which will always fall in cases of conditional instability. So, in summary, for large negative β_i we expect dry advantage, but for small negative β_i wet advantage is possible.

On occasions when the air within the boundary layer is drier than the higher layers into which it is growning, β_i is positive. In these circumstances, entrainment leads to an increase of θ_e in the boundary layer and a descent of the LFC. Consequently, there is strong dry advantage, with the boundary layer growing rapidly and the LFC descending over the dry surface. The dry advantage for $\beta_i > 0$ is apparent in Figure 3.

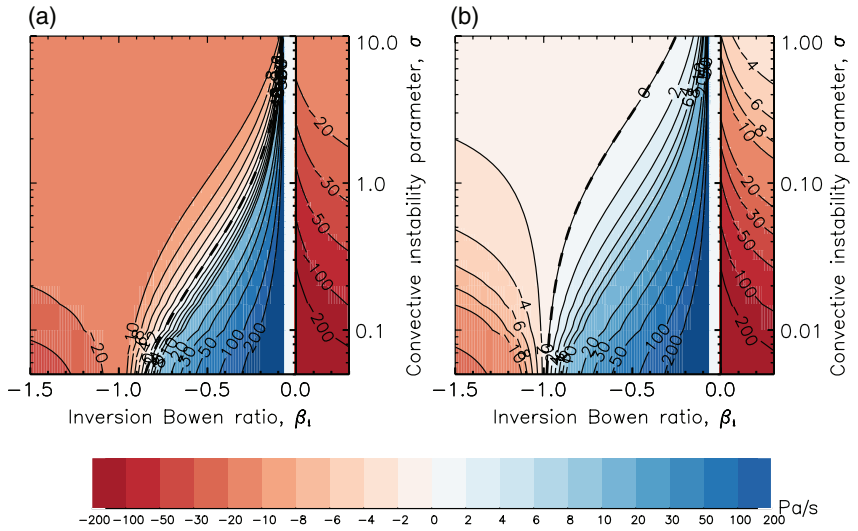

FIGURE 3 Example plots of ΔR, the magnitude of the sensitivity of convective triggering rate to surface Bowen ratio, as a function of inversion Bowen ratio β_i and convective instability parameter σ, for (a) $\Gamma_+ = 10^{-4}$ K/Pa, and (b) $\Gamma_+ = 10^{-3}$ K/Pa. The separatrix between wet and dry advantage is indicated with a bold dashed line: note that this line is identical in each panel, but the axis scalings are different, to reflect the different ranges of σ appropriate in each case. For negative β_i, the most common state, wet advantage occurs below the separatrix and dry advantage above. The region of $\beta_v < \beta_i < 0$ corresponds to an unstable boundary-layer top and is shown as white. Postive β_i corresponds to strong dry advantage

It has already been noted that the convective instability parameter, $\sigma = S_F/\Gamma_+$, corresponds to a measure of lower tropospheric instability, since S_F is a measure of conditional instability and σ decreases with both Γ_+ and Γ_F. σ also represents the degree to which p_F and P_i are responsive to the surface heat fluxes and attendant changes in PBL thermodynamics and could be termed a "stiffness ratio". If S_F is high, then the LFC is in some sense "stiff" in relation to the changes in θ_e in the boundary layer, meaning that the descent of the LFC with increasing boundary layer θ_e is slow. If Γ_+ is high, then the PBL grows relatively slowly over both wet and dry surfaces. Therefore, if the convective instability parameter, σ, is high, the LFC remains relatively fixed while the PBL is more mobile and may grow more rapidly (particularly over dry surfaces, where sensible heating is significant). In contrast, if σ is low, the LFC moves more freely in response to PBL θ_e, but the boundary-layer depth grows more slowly; in these circumstances wet advantage is possible.

Combining the effects of the controlling parameters, we find wet advantage to be increased when β_i is small negative and when σ is low (below the separatrix curve in Figure 3). In this case, p_F descends rapidly over the wet surface and is also more highly sensitive to θ_e in the PBL. θ_e is lower over a dry than a wet surface, and therefore p_F is also lower (higher altitude) over the dry. It should also be remembered that the situation of low σ corresponds to high dry stability in the lower troposphere and relatively high static stability around the LFC, and may be too stable for deep convection to occur at all.

3.4 | Amplitude and sign of R: is wet or dry advantage significant?

It has been seen that the possibility of wet or dry advantage is determined by the separatrix curve in Figure 3, but for any advantage to be significant we still require the sensitivity of R to the Bowen ratio, ΔR, to be large. We can say that ΔR, which is proportional to $R_1(b+a)$, will be large in magnitude when the magnitude of $(b+a)$ is large and/or R_1 is large.

If Γ_+ is large (meaning lower R_1 and lower σ), CBL growth is slow over both wet and dry surfaces. In this case, there is little entrainment of dry air from aloft over either surface and the development of θ_e and LFC is very similar over the wet and dry. Consequently, there can only be weak advantage between wet and dry surfaces.

The rate parameter, R_1, also depends on the net heat flux, F_n: the rates of PBL growth and θ_e tendency are controlled by the magnitude of surface fluxes; if these fluxes are weak then R_1 is small and there will be little tendency for convective development through this one-dimensional process. Similarly, the dependence of R_1 on P_i can be explained quite easily: when P_i is small, the rate of boundary-layer growth is much more rapid (heat is added to a smaller mass) and therefore there can be much greater difference between wet and dry environments.

We require R to be significantly negative somewhere, for any advantage between dry and wet surfaces to be significant. In considering this, we treat the regions of dry and wet advantage separately and consider the possible curves in Figure 2.

- In regions of wet advantage, we require $R(0) = -R_1 a$ to be large and negative for R to be sufficiently negative over a wet surface.
- In regions of dry advantage, we require $R(\infty) = R_1 b$ to be large and negative, which only fails when β_i is very small and negative (in which case we expect wet advantage anyway).

These conditions were tested in the plotting of Figure 3 and the condition of large negative R in in cases of wet or dry advantage was always fulfilled.

Finally, note that there is a connection between the conditions on σ and R_1, in that inversion stability Γ_+ appears in both parameters, in ways that are in opposition. High Γ_+ will tend to decrease σ, generally increasing the likelihood of wet advantage by suppressing vertical growth of the boundary layer over the dry surface. At the same time, high Γ_+ will also decrease R_1 and will therefore tend to reduce the amplitude of this wet advantage, by suppressing boundary-layer growth also.

4 | DISCUSSION OF THE THEORETICAL FRAMEWORK

4.1 | Relationship to previous solutions

While FE03a proposed that the tendency of deep convective initation is controlled by two parameters, CTP and HI, we find the dynamics of the system to depend on three parameters. Only two parameters, β_i and σ, determine the separatrix between wet and dry advantage (namely $(a + b) = 0$, plotted in Figure 3), but this is not a sufficient condition and it is also necessary that $R_1(a + b)$ is large enough in Equation 17, in order for any advantage to exist, and therefore the third, dimensional parameter, R_1 cannot be neglected. Gentine *et al.* (2013), who used a different approach to analysing the same system, present their solutions in terms of four controlling parameters, namely the profile stability (our Γ_+), evaporative fraction, tropospheric relative humidity, and potential temperature. Our approach has therefore reduced the number of free parameters; for instance, the nondimensional β_i and σ are sensitive to the temperature and humidity.

The CTP measure defined by FE03a can be considered as a measure of instability above the CBL inversion and, broadly, we can associate high CTP with both lower Γ_+ and higher S_F, meaning a high convective instability parameter, σ. FE03a found that higher CTP (broadly associated with higher σ) led to a greater likelihood of dry advantage (for sufficiently high HI). Here, we confirm that higher σ does favour dry advantage. High CTP, in corresponding to decreased Γ_+, will also increase the strength of the advantage between dry and wet (through R_1 in Equation 17). Therefore, in regard to CTP and its approximate relationship with σ and R_1, the results derived here are in accord with those of FE03a.

Gentine *et al.* (2013) also indicate that low tropospheric stability leads to dry advantage, at least in conditions of reasonably warm and humid tropospheric conditions. For a cool and humid tropospheric profile, Gentine *et al.* (2013) show that wet advantage occurs increasingly with increasing stability: these conditions correspond to low σ and small negative β_i and are therefore apparently consistent with our solutions. Similarly, our results are broadly consistent with those of Yin *et al.* (2015), who found dry advantage to occur with low tropospheric stability and low (negative) vertical gradient of specific humidity (which we may associate with strongly negative β_i).

Where FE03a used HI as a sum of the humidities (dewpoint depressions) in the boundary layer and the layer immediately above it, our analysis, as well as that of Yin *et al.* (2015), highlights the importance of the *difference* in humidities between these layers, as expressed in the inversion Bowen ratio β_i. The inversion Bowen ratio controls the evolution of θ_e as a boundary layer grows vertically, and therefore it controls the behaviour of p_F. FE03a assumed that in conditions of high surface Bowen ratio, when the boundary layer is growing rapidly, the LFC remains fairly constant in height and dry advantage is likely. However, when β_i is small and negative, the LFC may also move upwards over the dry surface, so that dry advantage is reduced.

4.2 | Limitations

In applying these results to real-world situations, a number of important limitations must be considered. The model is restricted to describing initiation of convective systems through daytime growth of the convective boundary layer, and not the important class of convective rainfall events occurring at night, nor convective events dynamically triggered, at cold fronts for instance. Guillod *et al.* (2014) highlight the role of synoptic forcing of rainfall in forcing a serial correlation of rainfall with soil moisture, regardless of any physical feedback between them. The distribution of rainfall by organized convective systems (MCSs) is also not likely to be captured by this model: such systems usually involve intense mesoscale flows (gravity currents and gravity waves), which trigger convection dynamically, somewhat independent of the underlying boundary-layer state. For these reasons, there is evidence that MCSs deliver more precipitation to a surface of low Bowen ratio, where there is simply more water vapour in the boundary layer available for precipitation (Clark *et al.*, 2003; Hartley *et al.*, 2016).

An additional, and fundamental, drawback of the model presented here is that its one-dimensional setup ignores mesoscale dynamic flows, which are also driven by differences in the boundary-layer state over adjacent wet and dry surfaces. Guillod *et al.* (2015) showed that we need to consider temporal and spatial relationships between rainfall and soil moisture separately and these relationships can be of the opposite sign. This being acknowledged, if we are concerned with the spatial distributions of rainfall and its role in either increasing or decreasing soil moisture heterogeneity, then the very question of whether wet or dry surfaces trigger convection first in a given atmospheric profile implies that these surfaces are in some proximity and therefore will tend to drive their own circulations on the boundaries. Such flows have been shown in observational (Taylor *et al.*, 2007; Kang *et al.*, 2007; Dixon *et al.*, 2012) and modelling (Garcia-Carreras *et al.*, 2011; Huang and Margulis, 2013; Rieck *et al.*, 2014) work to be significant in modifying the thermodynamic distributions under conditions of reasonably light winds. Rochetin *et al.* (2017) used a model to analyse

in detail how the boundary-layer thermodynamics evolve in the pre-convective hours and are influenced by large-scale and mesoscale advection, which conditions the entrainment and surface flux regimes to be much more complex than a one-dimensional model can easily encompass. The mesoscale circulations are thermally direct, with hot air rising, and tend to give the greatest convective triggering on the warm and dry side of a surface boundary (specifically, on the downwind side of a warm/dry surface). Garcia-Carreras *et al.* (2011) also showed that this location is where, due to interactions of mixing and advection, the boundary-layer θ_e is maximized, giving an additional advantage for convective triggering close to the boundaries. Taylor *et al.* (2012), in a global analysis, found dry advantage at almost every location where a significant signal appeared and argued that this is consistent with dynamic triggering on the warm side of boundaries. Situations where the one-dimensional model may best apply might be those where the boundaries between contrasting wet and dry surfaces are relatively smooth transitions, meaning that pressure gradients and the resulting circulations may be weak.

One uncertainty in the method developed here is that it is (like FE03a) based on the morning thermodynamic profile and does not follow the full transition through several hours towards the eventual point of convective initiation. A number of functions of the system will necessarily change during this evolution, differently over wet and dry surfaces, including the surface and inversion Bowen ratios, β and β_i. In contrast, the approach of Gentine *et al.* (2013) was to integrate the basic equations through the day and inspect the conditions that would prevail by sunset: this method introduces similar uncertainties, notably that the tendency is consistent between wet and dry surfaces over this longer time period. The analysis shown here indicates the sense of the tendency towards deep convection in the morning, but does not tell us whether that tendency is maintained consistently in the following hours. Whether the method does consistently capture wet and dry advantage must be tested in practice. Note that use of a single morning profile can also be regarded as a significant benefit of this approach, because it leads to a system that is relatively straightforward to apply and interpret in practical applications, requiring only a morning sounding.

Finally, the practical application of the theoretical model will depend on obtaining appropriate profile and land-surface data to which it can be applied. Guillod *et al.* (2014) showed the difficulties of obtaining good surface data, while observational profiles are often not available on the spatial scales needed for boundary-layer analysis and can involve significant errors in the convective boundary layer, due to their sampling of transient eddies (Weckwerth *et al.*, 1996).

Ultimately, the question of whether this, or any other one-dimensional model, can usefully describe real convective initiation regimes will only be answered by testing on observations and numerical models. A first attempt to evaluate the theoretical framework with convection-permitting model data is described in the next section.

5 | FRAMEWORK EVALUATION

A comprehensive evaluation of the theoretical model is beyond the scope of this article. Guillod *et al.* (2014) explain some of the many difficulties in effectively diagnosing soil-moisture relationships with rainfall from observations. These difficulties include uncertainties in surface flux data and difficulties in separating external forcing of serial correlations of soil moisture with rainfall, for instance due to synoptic forcing, from direct physical coupling. Rather than attempt to use measurements to evaluate the theoretical framework, here we make a first attempt to show how it may be applied in practice, by using the framework to analyse results from a convection-permitting numerical model simulation performed over India. A study of similar model simulations applied in the Sahel region of Africa (*Cascade* project: Taylor *et al.*, 2013) has shown that a convection-permitting simulation at 4 km resolution can exhibit excellent spatial relationships between soil moisture and convective triggering, similar to those inferred from observational proxy data (including aircraft-based case studies and statistical analysis of satellite data).

5.1 | EMBRACE simulation and data

Diagnostics from a limited-area model simulation of the Met Office Unified Model (Met UM), run as part of the Earth system Model Bias Reduction and assessing Abrupt Climate change (EMBRACE) project, are used for this study. A model run with 4 km grid spacing over a large domain containing the entire Indian subcontinent has been considered. The 4 km resolution model uses non-parametrized (explicit) convection and a 3D Smagorinsky scheme for sub-grid mixing. The model was initialized on August 18, 2011 at 0000 UTC with the Met Office global operational analysis flow fields and run for 21 days. Lateral boundary conditions were updated every hour and derived from a series of six-hour long global MetUM simulations run from each successive operational analysis, which is available every 6 hr. The soil moisture was initialized by downscaling the soil moisture of the global model analysis. The soil moisture stress was kept the same as in the global model, meaning that the soil moisture in the high-resolution model is different from that in the global one, because of the more detailed soil properties of the high-resolution model. The EMBRACE simulation configuration is described in more detail by Willetts *et al.* (2017), who also show that the rainfall distributions in the model verify well against satellite-derived rainfall estimates for most parts of India.

5.2 | Study domain and convective precipitation initiation

In analysing the initiation of deep convection in the EMBRACE simulations, four subdomains have been used (shown in Figure 4). The northern and southern domains are arid to semi-arid in climatic conditions, whereas the central

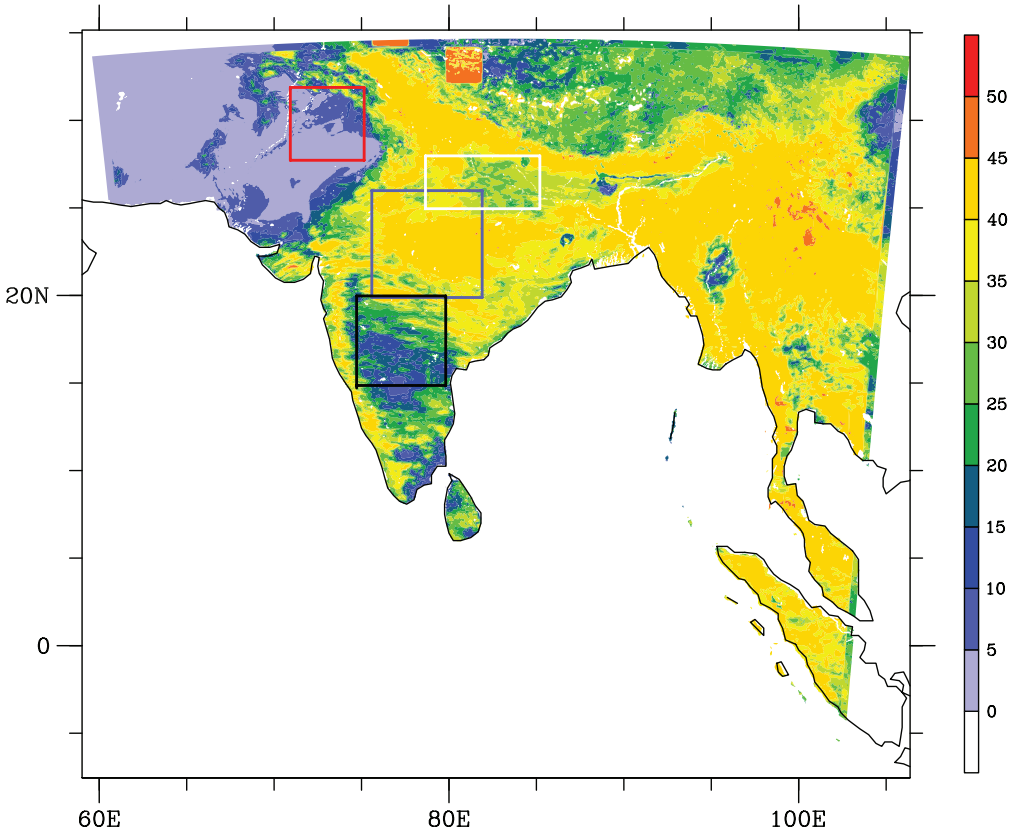

FIGURE 4 Map of daily surface soil moisture (kg/m^2) for a single date in the model simulation, August 21, 2011, overlaid by the study domains: (a) northern (red), (b) eastern (white), (c) centre (blue), and (d) southern (black)

and eastern domains have more humid conditions. The northern, central and eastern study domains lie along the axis of the monsoon trough, whereas the southern domain is positioned a little off track. Therefore these four domains encapsulate a range of climatic conditions typical of the Indian monsoon. We have studied only those initiations where the difference between the 90th and 10th percentiles of orographic height is less than 300 m, to discard orographically induced rainfall (following Taylor *et al.*, 2011).

An afternoon rain event is diagnosed with a method similar to Taylor *et al.* (2013) using hourly accumulated precipitation between 1130 and 2030 LT (where Local Time (LT) is UTC plus 5.5 hr). An afternoon rainfall event is defined where there is no rainfall in the chosen area in the 3 hr preceding 1130 LT (to remove stratiform rainfall events, which continue from overnight). The first step in the method is to identify a contiguous rain area (Ebert and McBride, 2000) using the flood-fill algorithm and thresholding technique. The minimum number of pixels to define a rain event as significant in this study is considered as 3 pixels, corresponding to 48 km^2. The minimum rain threshold for all the domains is taken as 3 mm accumulated rain in one hour. Then, the location of initiations is traced back in time to a single grid point, using 10-minute accumulated rainfall. Over the subdomains used, 1,688 intiations were thereby identified with the method.

5.3 | Computation of profile parameters

The theoretical framework has been evaluated using early morning profiles at 0300 UTC from the 4 km EMBRACE simulation. For all parts of the subdomains, this is after sunrise and before 0900 local time, meaning that we are able to analyse the shallow, early-morning convective boundary layer. We have computed β_i, σ and the resulting ΔR, via Equations 20 and 21, from the EMBRACE output for afternoon convective initiations within the four defined domains.

Computation of S_F is a two-stage process. First, the LFC is determined through computation of the moist ascent (Normand's construction) of a boundary-layer parcel: here LFC is the level where the parcel saturated ascent profile meets the environment profile and this computation is a standard element in routines to compute CAPE, for instance. Once the LFC is identified, S_F is computed as the vertical gradient of θ_{es}, using Equation 25. In practice, there are complexities in this calculation. The precise value of S_F at the LFC may be very sensitive to local thermodynamic anomalies in the profile. Also, sometimes during the morning the LFC does not exist and only appears later in the morning. For instance, in the EMBRACE data, out of 1,688 initiations, the LFC exists for only 783 cases in the 0300 UTC profile. Thus, we applied bulk estimates of relatively broad layers between fixed pressure levels to compute S_F. Analysis of the distributions of the PBL top and LFC (not shown) indicates that the inversion height (PBL top) has quite a narrow range between

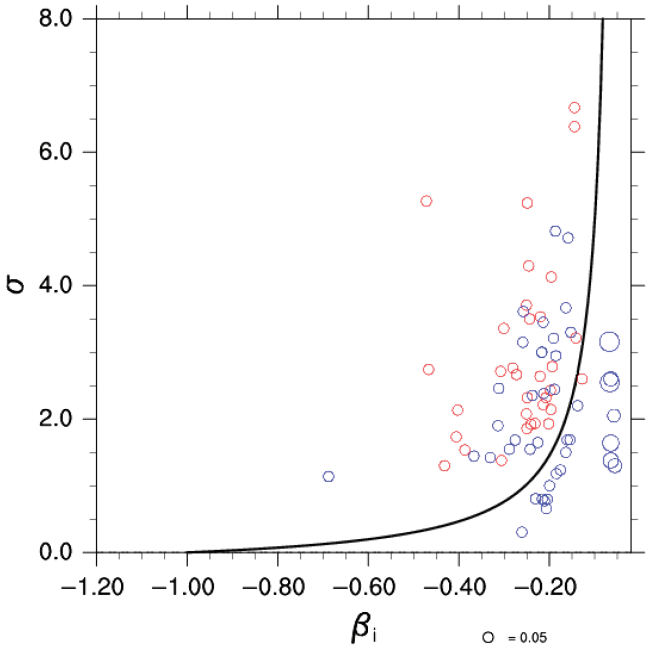

FIGURE 5 Reconstruction of Figure 3 for initiations diagnosed in the EMBRACE simulation. Wet (blue) and dry (red) circles represent actual soil moisture conditions at the location of initiation. The size of each circle denotes the magnitude of ΔR, and only those events for which $R < 0$ and $\Delta R \geq 0.05$Pa/s (indicated in the key) are included. The black line is the theoretical separatix curve

875 and 975 hPa, whereas the LFC can take a wide range of values, falling mostly within the range 550–850 hPa. Thus in computing bulk estimates of LFC we have chosen 550 and 850 hPa as reference levels and computed mean gradients between these levels.

To find β_i and Γ_+ is also a two-stage process. First, the convective boundary-layer inversion level is identified as the first level at which boundary-layer air is negatively buoyant. In practice, the inversion is not always easy to define precisely in early-morning profiles, when the boundary layer may be shallow: if the local sounding is too early, say 0000 UTC over India, which is just around sunrise, there may be no convective layer at all. However, in the 0300 UTC soundings used here, 1,467 of the 1,688 profiles had a clear inversion identified with this method. Furthermore, gradients in the thermodynamic parameters above the inversion can also lead to some ambiguity. Here, β_i has been computed based on the differences in specific humidity and potential temperature using the nearest possible layers across the inversion level, using Equation 23. Γ_+ is then computed as the vertical gradient of θ just above the capping inversion.

5.4 | Results of the framework evaluation

A subset of the convective initiations diagnosed in the simulation is plotted in Figure 5. In order to test the theoretical framework, we only include those initiations for which a significant difference between wet and dry advantage is predicted ($\Delta R \geq 0.05$ Pa/s) and for which the actual underlying surface was very wet or dry. The colour of the points denotes the actual surface conditions at the location of initiation: red implies an evaporative fraction less than 0.3 and blue shows an evaporative fraction greater than 0.9. Of the 1,681 initiations in the simulation, 74 occur in these conditions of low or high evaporative fraction and significant ΔR and are plotted in (β_i, σ) space.

Figure 5 indicates that the probability of rain initiation over a dry surface (red points) was almost exactly predicted with the theoretical model: nearly all of the 33 dry-surface initiations lie above the wet–dry separatrix curve. In contrast, wet initiations have mixed results. While, for large ΔR, wet-surface initiation events did occur in conditions successfully predicted to be wet (large blue points below the separatrix), for weaker ΔR, a significant number of wet-surface initiations had been predicted by the theoretical model to be over a dry surface (smaller blue points above the separatrix). It is likely that these smaller blue points in the dry region are cases in which the surface-forced advantage is weak (small ΔR) and there is significant external forcing for the convective trigger, either by dynamical forcing or by coherent topological control. For instance, the observational study of Guillod *et al.* (2014) for regions of the United States found that precipitation the previous day was a better predictor of afternoon rainfall than surface state, implying that external drivers dominated the initiation in these examples. In cases where an external dynamical forcing controls the initiation, it is usually expected that initiations will occur first at the location where there is greatest moist static energy, usually over a wet surface (for example, Clark *et al.*, 2003; Guillod *et al.*, 2014; Hartley *et al.*, 2016).

In conclusion, the results from the EMBRACE simulation provide support for the use of the theoretical model, in that it seems able to identify the conditions under which dry initiation is to be expected. Further analysis would be needed to establish the performance of the model for wet initiations, and in particular to separate local, thermodynamic initiation from dynamically forced initiation in the data.

6 | CONCLUSIONS

We have developed a thermodynamic model that describes the evolution of an atmospheric profile towards deep convective triggering, according to the underlying surface fluxes over wetter or drier surfaces. The model is derived from fundamental equations for boundary-layer and convective physics and leads to analytical solutions. The equations describe the relative effects of deepening of the convective boundary layer (which is faster over a dry surface) and the lowering of the LFC (which is faster over a wet surface), and the outcome can yield "wet advantage" (positive feedback) or "dry advantage" (negative feedback), depending on the profile. This one-dimensional model can be applied in atmospheric

conditions of relatively weak dynamical forcing. For these circumstances, our results are a compact solution, derived from sound physical equations, to the conceptual framework proposed by FE03a, which has been widely used.

Unlike FE03a, we find the system to be governed by three parameters. However, fortunately, only two of these are needed to separate the possible conditions of wet and dry advantage. These two parameters are β_i, the inversion-level Bowen ratio, and the convective instability parameter, σ. Together, β_i and σ define the separatrix curve shown in Figure 3. Dry advantange (negative feedback of rainfall with soil moisture) is favoured when σ is high and β_i is either large and negative, or positive. In this situation, the LFC is relatively insensitive to the boundary-layer conditions and the rapid growth of the boundary layer over a dry surface gives convective advantage. Wet advantage (positive feedback) is predicted when σ is low (a stable lower troposphere) and β_i is small and negative, meaning dry conditions above the boundary layer and strong drying of the boundary layer by entrainment. In these circumstances, the small values of β_i imply dry conditions above the boundary layer, leading to drying of the boundary layer by entrainment, which reduces the likelihood of deep convection over a dry surface for which the boundary-layer growth is rapid. Although the separatrix divides conditions of wet or dry advantage, whether this advantage is relevant depends on the amplitude of the signal and, in order to determine this amplitude, all three controlling parameters need to be taken into account. One attractive feature of the model developed here is that its two parameters determining the sign of the solution, σ and β_i, are nondimensional, with no free parameters needing calibration according to climatic conditions. Note that articles applying the FE03a method to different climatic regions have expressed a need to change the parameter regimes accordingly (Ferguson and Wood, 2011; Tuinenberg *et al.*, 2011). When parameters are dependent on the climatic conditions, the application of a model for extrapolation to new areas, or to future climates, is questionable.

While a comprehensive evaluation of the theoretical model is beyond the scope of this article, the model has been tested here against convection-permitting numerical model simulations. The results of the testing indicate that the model may indeed be effective, particularly in the diagnosis of conditions for dry advantage (rainfall over dry surfaces). Wet advantage cases were not effectively separated by the model; quite likely, this is related to those events being controlled by dynamical forcing of the convection, in which case initiation over wetter surfaces is generally expected. Further testing of the model beyond these first steps is certainly needed. The equations provided in this article provide a quantitative prediction of the possibility of wet or dry advantage occurring systematically, which is a question of great importance to climatic analysis and to weather and climate prediction, especially over areas where water availability is critical to human livelihoods.

ACKNOWLEDGEMENTS

D.J.P. is supported by a Royal Society Wolfson Research Merit Award, and M.B. has been supported by a Commonwealth PhD Scholarship (INCS-2012-161). This work was also supported by the AMMA-2 (NERC NE/G018499/1), AMMA-2050 (DFID-NERC NE/M020126/1), IMPALA (DFID-NERC NE/M017176/1), VERA (NERC NE/M00 3574/1), and INCOMPASS (NERC NE/L013843/1) projects. The EMBRACE simulations were performed by Stuart Webster at the Met Office, who also provided assistance in their analysis. We are grateful to John Marsham, Luis Garcia-Carreras, and Andy Ross for helpful discussions and to the anonymous reviewers, whose suggestions significantly improved the presentation of the results.

REFERENCES

Betts, A.K. (1973) Non-precipitating cumulus convection and its parameterization. *Quarterly Journal of the Royal Meteorological Society*, 99, 178–196.

Betts, A.K. (1992) FIFE atmospheric boundary layer budget methods. *Journal of Geophysical Research*, 97, 18,523–18,531.

Betts, A.K. and Ball, J.H. (1995) The FIFE surface diurnal cycle climate. *Journal of Geophysical Research*, 100, 25,679–25,693.

Birch, C.E., Parker, D.J., O'Leary, A., Marsham, J.H., Taylor, C.M., Harris, P.P. and Lister, G.M.S. (2013) Impact of soil moisture and convectively generated waves on the initiation of a west African mesoscale convective system. *Quarterly Journal of the Royal Meteorological Society*, 139, 1712–1730. https://doi.org/10.1002/qj.2062.

Birch, C.E., Marsham, J.H., Parker, D.J. and Taylor, C.M. (2014) The scale dependence and structure of convergence fields preceding the initiation of deep convection. *Geophysical Research Letters*, 41, 4769–4776. https://doi.org/10.1002/2014GL060493.

Carson, D.J. (1973) The development of a dry inversion-capped convectively unstable boundary layer. *Quarterly Journal of the Royal Meteorological Society*, 99, 450–467.

Chen, F. and Avissar, R. (1994) The impact of land-surface wetness heterogeneity on mesoscale heat fluxes. *Journal of Applied Meteorology*, 33, 1323–1340.

Clark, D.B., Taylor, C.M., Thorpe, A.J., Harding, R.J. and Nicholls, M.E. (2003) The influence of spatial variability of boundary-layer moisture on tropical continental squall lines. *Quarterly Journal of the Royal Meteorological Society*, 129, 1101–1121. https://doi.org/10.1256/qj.02.122.

Cutrim, E., Martin, D.W. and Rabin, R. (1995) Enhancement of cumulus clouds over deforested lands in Amazonia. *Bulletin of the American Meteorological Society*, 76(10), 1801–1805. https://doi.org/10.1175/1520-0477(1995)076<1801:EOCCOD>2.0.CO;2.

Daly, E., Porparato, A. and Rodriguez-Iturbe, I. (2004) Coupled dynamics of photosynthesis, transpiration, and soil water balance: part II. Stochastic analysis and ecohydrological significance. *Journal of Hydrometeorology*, 5, 559–566.

Dixon, N.S., Parker, D.J., Garcia-Carreras, L., Taylor, C.M., Harris, P.P., Marsham, J.H., Polcher, J. and Woolley, A. (2012) The effect of background wind on mesoscale circulations above variable soil moisture in the Sahel. *Quarterly Journal of the Royal Meteorological Society*, 1009–1024. https://doi.org/10.1002/qj.2012.

Ebert, E.E. and McBride, J. (2000) Verification of precipitation in weather systems: determination of systematic errors. *Journal of Hydrology*, 239, 179-202. https://doi.org/10.1016/S0022-1694(00)00343-7.

Ek, M.B. and Holtslag, A.A.M. (2004) Influence of soil moisture on boundary-layer cloud development. *Journal of Hydrometeorology*, 5, 86–99. https://doi.org/10.1175/1525-7541(2004)005<0086:IOSMOB>2.0.CO;2.

Eltahir, E.A.B. (1998) A soil moisture rainfall feedback mechanism 1. Theory and observations. *Water Resources Research*, 34, 765–776. https://doi.org/10.1029/97WR03499.

Ferguson, C.R. and Wood, E.F. (2011) Observed land–atmosphere coupling from satellite remote sensing and reanalysis. *Journal of Hydrometeorology*, 12, 1221–1254. https://doi.org/10.1175/2011JHM1380.1.

Findell, K.L. and Eltahir, E.A.B. (2003) Atmospheric controls on soil moisture – boundary layer interactions. Part I: framework development. *Journal of Hydrometeorology*, 4, 552–569.

Garcia-Carreras, L., Parker, D.J., Taylor, C.M., Reeves, C.E. and Murphy, J.G. (2010) Impact of mesoscale vegetation heterogeneities on the dynamical and thermodynamic properties of the planetary boundary layer. *Journal of Geophysical Research, Atmospheres*, 115, D03102. https://doi.org/10.1029/2009JD012811.

Garcia-Carreras, L., Parker, D.J. and Marsham, J.H. (2011) What is the mechanism for the modification of convective cloud distributions by land surface-induced flows? *Journal of the Atmospheric Sciences*, 68, 619–634. https://doi.org/10.1175/2010JAS3604.1.

Gentine, P., Holtslag, A.A.M., D'Andrea, F. and Ek, M. (2013) Surface and atmospheric controls on the onset of moist convection over land. *Journal of Hydrometeorology*, 14, 1443–1462.

Guillod, B.P., Orlowsky, B., Miralles, D.G., Teuling, A.J., Blanken, P.D., Buchmann, N., Ciais, P., Ek, M., Findell, K.L., Gentine, P., Lintner, B.R., Scott, R.L., Van den Hurk, B. and Seneviratne, S.I. (2014) Land-surface controls on afternoon precipitation diagnosed from observational data: uncertainties and confounding factors. *Atmospheric Chemistry and Physics*, 14, 8343–8367.

Guillod, B.P., Orlowsky, B., Miralles, D.G., Teuling, A.J. and Seneviratne, S.I. (2015) Reconciling spatial and temporal soil moisture effects on afternoon rainfall. *Nature Communications*, 6, 6443.

Haiden, T. (1997) An analytical study of cumulus onset. *Quarterly Journal of the Royal Meteorological Society*, 123, 1945–1960.

Hartley, A.J., Parker, D.J., Garcia-Carreras, L. and Webster, S. (2016) Simulation of vegetation feedbacks on local and regional scale precipitation in West Africa. *Agricultural and Forest Meteorology*, 222, 59–70. https://doi.org/10.1016/j.agrformet.2016.03.001.

Huang, H.-Y. and Margulis, S.A. (2010) Evaluation of a fully coupled large-eddy simulation–land surface model and its diagnosis of land–atmosphere feedbacks. *Water Resources Research*, 46, W06512. https://doi.org/10.1029/2009WR008232.

Huang, H.-Y. and Margulis, S.A. (2011) Investigating the impact of soil moisture and atmospheric stability on cloud development and distribution using a coupled large-eddy simulation and land surface model. *Journal of Hydrometeorology*, 12, 787–804.

Huang, H.-Y. and Margulis, S.A. (2013) Impact of soil moisture heterogeneity length scale and gradients on daytime coupled land–cloudy boundary layer interactions. *Hydrological Processes*, 27, 1988–2003. https://doi.org/10.1002/hyp.9351.

Kang, S.-L., Davis, K.J. and LeMone, M. (2007) Observations of the ABL structures over a heterogeneous land surface during IHOP_2002. *Journal of Hydrometeorology*, 8, 221–244.

LeMone, M.A., Grossman, R.L., Coulter, R.L., Wesley, M.L., Klazura, G.E., Poulos, G.S., Blumen, W., Lundquist, J.K., Cuenca, R.H., Kelly, S.F., Brandes, E.A., Oncley, S.P., McMillen, R.T. and Hicks, B.B. (2000) Land–atmosphere interaction research, early results, and opportunities in the Walnut River watershed in Southeast Kansas: CASES and ABLE. *Bulletin of the American Meteorological Society*, 81, 757–779. https://doi.org/10.1175/1520-0477(2000)081<0757:LIRERA>2.3.CO;2.

Lintner, B.R., Gentine, P., Findell, K.L., D'Andrea F, Sobel AH and Salvucci GD (2013) An idealized prototype for large-scale land–atmosphere coupling. *Journal of Climate*, 26, 2379–2389. https://doi.org/10.1175/JCLI-D-11-00561.1.

Parker, D.J. (2002) The response of CAPE and CIN to tropospheric thermal variations. *Quarterly Journal of the Royal Meteorological Society*, 128, 119–130.

Parsons, D.B., Yoneyama, K. and Redelsperger, J.L. (2000) The evolution of the tropical western Pacific atmosphere–ocean system following the arrival of a dry intrusion. *Quarterly Journal of the Royal Meteorological Society*, 126, 517–548. https://doi.org/10.1256/smsqj.56306.

Pielke, R.A. (2001) Influence of the spatial distribution of vegetation and soils on the prediction of cumulus convective rainfall. *Reviews of Geophysics*, 39, 151–177.

Pielke, R.A., Dalu, G.A., Snook, J.S., Lee, T.J. and Kittel, T.G.F. (1991) Nonlinear influence of mesoscale land use on weather and climate. *Journal of Climate*, 4, 1053–1069.

Pielke, R.A., Lee, T.J., Copeland, J.H., Eastman, J.L., Ziegler, C.L. and Finle, C.A. (1997) Use of USGS-provided data to improve WEATHERAND climate simulations. *Ecological Applications*, 7, 3–21. https://doi.org/10.1890/1051-0761(1997)007[0003:UOUPDT]2.0.CO;2.

Rieck, M., Hohenegger, C. and van Heerwaarden, C.C. (2014) The influence of land surface heterogeneities on cloud size development. *Monthly Weather Review*, 142, 3830–3846.

Rochetin, N., Couvreux, F. and Guichard, F. (2017) Morphology of breeze circulations induced by surface flux heterogeneities and their impact on convection initiation. *Quarterly Journal of the Royal Meteorological Society*, 143, 463–478. https://doi.org/10.1002/qj.2935.

Schär, C., Lüthi, D., Beyerle, U. and Heise, E. (1999) The soil-precipitation feedback: a process study with a regional climate model. *Journal of Climate*, 12, 722–741.

Taylor, C.M. and Ellis, R.J. (2006) Satellite detection of soil moisture impacts on convection at the mesoscale. *Geophysical Research Letters*, 33, L03404. https://doi.org/10.1029/2005GL025252.

Taylor, C.M., Parker, D.J. and Harris, P.P. (2007) An observational case study of mesoscale atmospheric circulations induced by soil moisture. *Geophysical Research Letters*, 34, L15801. https://doi.org/10.1029/2007GL030572.

Taylor, C.M., Gounou, A., Guichard, F., Harris, P.P., Ellis, R.J., Couvreux, F. and De Kauwe, M. (2011) Frequency of Sahelian storm initiation enhanced over mesoscale soil-moisture patterns. *Nature Geoscience*, 4, 430–433. https://doi.org/10.1038/ngeo1173.

Taylor, C.M., de Jeu, R.A.M., Guichard, F., Harris, P.P. and Dorigo, W.A. (2012) Afternoon rain more likely over drier soils. *Nature*, 489(7416), 423–426. https://doi.org/10.1038/nature11377.

Taylor, C.M., Birch, C.E., Parker, D.J., Dixon, N., Guichard, F., Nikulin, G. and Lister, G.M.S. (2013) Modeling soil moisture-precipitation feedback in the Sahel: importance of spatial scale versus convective parameterization. *Geophysical Research Letters*, 40, 6213–6218. https://doi.org/https://doi.org/10.1002/2013GL058511.

Tennekes, H. (1973) A model for the dynamics of the inversion above a convective boundary layer. *Journal of the Atmospheric Sciences*, 30, 558–567.

Trier, S.B., Chen, F. and Manning, K.W. (2004) A study of convection initiation in a mesoscale model using high-resolution land surface initial conditions. *Monthly Weather Review*, 132, 2954–2976. https://doi.org/10.1175/MWR2839.1.

Tuinenburg, O.A., Hutjes, R.W.A., Jacobs, C.M.J. and Kabat, P. (2011) Diagnosis of local land–atmosphere feedbacks in India. *Journal of Climate*, 24, 251–266.

Wang, J.F., Chagnon, F.J.F., Williams, E.R., Betts, A.K., Renno, N.O., Machado, L.A.T., Bisht, G., Knox, R. and Brase, R.L. (2009) Impact of deforestation in the Amazon basin on cloud climatology. *Proceedings of the National Academy of Sciences of the United States of America*, 106(10), 3670–3674. https://doi.org/10.1073/pnas.0810156106.

Weckwerth, T., Wilson, J.W. and Wakimoto, R.M. (1996) Thermodynamic variability within the convective boundary layer due to horizontal convective rolls. *Monthly Weather Review*, 124, 769–784. https://doi.org/10.1175/1520-0493(1996)124<0769:TVWTCB>2.0.CO;2.

Willetts, P.D., Marsham, J.H., Birch, C.E., Parker, D.J., Webster, S. and Petch, J. (2017) Moist convection and its upscale effects in simulations of the Indian monsoon with explicit and parametrized convection. *Quarterly Journal of the Royal Meteorological Society*, 143, 1073–1085. https://doi.org/https://doi.org/10.1002/qj.2991.

Yin, J., Albertson, J.D., Rigby, J.R. and Porporato, A. (2015) Land and atmospheric controls on initiation and intensity of moist convection: CAPE dynamics and LCL crossings. *Water Resources Research*, 51, 8476–8493. https://doi.org/10.1002/2015WR017286.

How to cite this article: Bhowmick M, Parker DJ. Analytical solution to a thermodynamic model for the sensitivity of afternoon deep convective initiation to the surface Bowen ratio. *Q J R Meteorol Soc.* 2018;144:2216–2229. https://doi.org/10.1002/qj.3340